

An Experimental and Analytical Study on Radial Shear of Reinforced Concrete Containments Under Pressure and Thermal Effects

J 4/12

Y. Aoyagi

*Central Research Institute of Electric Power Industry,
1646 Abiko, Abiko-shi, Chiba 270-11, Japan*

K. Okada

*Takenaka Technical Research Laboratory,
Takenaka Komuten Co., Ltd.,
5-14, 2-chome, Minamisuna, Tokyo 136, Japan*

N. Tanaka

*Shimizu Construction Co., Ltd., Research Laboratory,
4-17, Etchujima-3, Koto-ku, Tokyo 135, Japan*

Summary

This report describes the test results and the nonlinear finite element analysis on one-twelfth scale models of prototype reinforced concrete containment vessels. This experimental study was carried out to estimate the radial shear of shell wall at the junction of base mat subjected to pressure and thermal effects.

The test models are circular shell wall of limited height with thick base mat (inner radius: 166.6 cm, wall height: 150 cm, wall thickness: 15 cm and base mat thickness: 50 cm). Tests were carried out on three models. Model I and II for pressure tests are different from each other only in the amount of vertical reinforcement. Model III tested under the combination of the pressure and thermal effects has the same dimensions and reinforcements as Model II. Pressure and thermal load are applied to the shell wall with airtight rubber tubes and flexible electric heating panels mounted on inner surface of the models. To obtain radial shear at the junction of base mat from the equilibrium of hoop force and lateral pressure, the hoop stresses of circumferential bars were measured using tension load-cells installed in the vertical slits situated at diametrically opposite position of shell wall.

The resistance mechanism of shell wall to radial shear, failure mode to pressure and the reduction of residual shear stress due to thermal effects under combined action of pressure was made clear through the experimental study.

The analytical results with nonlinear finite element analysis considering the contribution of tensile stress of concrete between cracks showed good agreement with the test results.

1. Introduction

In general, a restraint of the free deformation of concrete containment at the junction of the base mat and the shell wall due to axisymmetric load such as LOCA pressure and thermal effects may give rise to a certain amount of radial shear stress in the wall bottom. In the previous report [1] the resistance mechanism of shear at the wall end against radial shear due to pressure was studied on the test models of an octant shell wall with the foundation mat which had a scale of one twelfth of the prototype of concrete containment vessels. From these experimental studies, the design criteria on radial shear in Japanese design code of containment vessel was proposed. Japanese code also specified in loading condition IV, where containment vessels are subjected to combined earthquake lateral force and thermal load effects, that the thermal effects can be neglected under this condition for safety analysis. The authors reported the experimental study on thermal effects with two scale models [2].

This experiment and analysis were carried out to confirm the proposed criteria on radial shear in Japanese code, which based on an octant circular shell wall models in previous test. Also, the authors tried to make clear the influence on radial shear strength due to thermal effects on failure mode and ultimate shear strength of wall end which could not enough investigated in previous study, and to confirm whether the criteria on thermal effects in loading condition IV in Japanese code is reasonable or not.

2. Test Models

The configurations and the main dimensions of the testing models were designed as shown in Fig. 1. They are circular shell wall having a limited height with thick base mat. The cylindrical wall of 15 cm thick and 150 cm high was fixed on to the base mat of 50 cm thick and the inner wall radius was 166.6 cm. The models had a scale of one-twelfth of the prototype containment vessel. The reinforcement ratio of wall and properties of material are listed in Table 1. The vertical reinforcement ratio of Model I was 1.11% which was two times larger than those of Model II and III. The circumferential reinforcement ratio of the specimens was all 0.88%. Normal sand and gravel concrete having the maximum aggregate size of 10 mm was used for the models. The compressive strength of concrete at the test was 240 kg/cm² for Model I and about 270 kg/cm² for Model II and III. Deformed bars of 10 mm in diameter were used for vertical and horizontal reinforcement. The yield strength was 3850 kg/cm², and the ultimate strength was 5700 kg/cm².

3. Test Method

3.1 Test Equipment: For pressurizing the inside surface of the wall outward radial direction, six water tubes (8 inches in diameter) made of clothing rubber were mounted between the wall and the reaction ring. Then pressure was applied by pumping the water into these tubes. The temperature of the wall in Model III was controlled by flexible electric heating panels mounted on inner surface of the model. To avoid the direct heat flow to pressurizing equipment, fiber glass mats were sandwiched between the pressure tubes and the heating panels as shown in Fig. 2. Two vertical slits located diametrically opposite were made in cylindrical wall but in Model III thin steel plates were installed instead of slits. The measurement of the radial shear force at the wall end was carried out by the load cells mounted on slits or thin separating plates.

In the pressure test in Models I and II, loading and unloading were repeated, ranging from elastic to concrete cracking and yielding of circumferential bars. Then the model was

brought to the ultimate state. The test program of Model III is shown in Fig. 3. The temperature at the inner wall was kept at 70°C and the thermal response of the model such as cracking formation, deformation and strains of reinforcement were measured. Finally, the model was pressurized until failure under the constant temperature condition. The hoop force of each couple of the circumferential bars was measured with the tension load-cells. The deformations of wall in radial direction were measured by dial gages and the strains of circumferential as well as vertical reinforcements were measured by electric wire strain gages.

4. Experimental Results

The summary of the experimental results are listed in Table 2.

4.1 Concrete Cracking: In Models I and II, initial vertical cracks were observed at the upper part of cylinder wall surface and then horizontal cracks developed at the mid-height of wall. From the pressure strain-curves of vertical reinforcements at the junction of the wall, it could be assumed that the horizontal cracks at the inner corner of the wall end occurred at 1.25 kg/cm² for Model I and at 1.6 kg/cm² for Model II. In Model III, the first visible signs of vertical cracks in the wall surface occurred when the temperature gradient of wall reached to 22.5 deg C. With further loading, circumferential cracks were also observed. However, the crack widths were less than 0.1 mm at the temperature gradient ΔT_g of 46 deg C which was maximum wall temperature gradient during the test period. These cracks developed along the bars and became wider during the pressure loading of the subsequent step.

4.2 Temperature distributions of Model III: The temperature difference between inner and outer surface of the wall, ΔT_g , and the difference of mean temperature of wall and base mat, ΔT_d , are also shown in Fig. 4. The temperature of the base mat was lower than other parts of the wall because of the heat flowing from the wall end to base mat.

4.3 Hoop Force - Distribution: Hoop forces of circumferential bars under pressure as well as under the combined load of pressure and thermal forces measured by the tensions load-cells are shown in Fig. 5 and Fig. 11. Yield of the circumferential bars occurred at around 3.0 kg/cm² and extended gradually downward from wall top. In Model III, the membrane compression force was introduced in the wall due to ΔT_d . Also, the difference between inner and outer force due to ΔT_g at the bar of same level was observed. With increase of pressure, the distribution of hoop forces became similar to that of Models I and II.

4.4 Ultimate Strength and Failure Modes: In the course of increasing the applied pressures, first the cracking at inner corner of wall end appeared prior to yield of circumferential bars of wall top. Then yielding of the vertical bars at the same points, and then yielding of circumferential bars also occurred at lower parts of the wall. Failure of Model I occurred at the circumferential bars at the top of the wall. In Models II and III, loading terminated at an pressure at 462 kg/cm² and at 5.0 kg/cm² respectively because of the difficulty in maintaining pressure which resulted from leakage of water from one of the pressure tubes. As shown in Table 2 the ultimate shear strength calculated by the equation from push off test [3] is slightly higher than experimental results. On the other hand it appeared that the predicted value from the proposed equation of Japanese concrete containment vessel code, which bases on resistance mechanism of circumferential bars against radial shear force [1], has enough safety margin against wall end design.

4.5 Transitions of Base Shear Stresses: In the loading condition where thermal effects,

ΔT_d , and lateral pressure, p , act to the wall, the equilibrium of radial components of membrane forces and the base shear of wall end is given by

$$h p + T + Q_p + Q_t = 0 \quad \text{eq. (1)}$$

where Q_p : base shear force due to pressure

Q_t : base shear force due to thermal effects ΔT_d

h : wall height

T is a sum of the radial components of hoop forces, calculated by the following equation.

$$T = \frac{1}{r} \int N_{\theta} dx \quad \text{eq. (2)}$$

where $N_{\theta} = N_p + N_t$, N_p and N_t are the membrane forces due to p and ΔT_g , respectively, r is radius of cylindrical wall. (See Fig. 6)

From equation (1) and (2), radial shear stress τ at the wall end is given by

$$\begin{aligned} \tau &= \frac{Q}{d} = \frac{h p}{d} - \frac{T}{dr} \\ &= \frac{h p}{d} - \frac{1}{dr} \int N_{\theta} dx \end{aligned} \quad \text{eq. (3)}$$

where d is the thickness of wall. The base shear stress is obtained by calculating T from such hoop force distribution as shown in Fig. 5 and putting it into equation (3).

The relationship between the radial shear at the wall end and lateral pressure of each model are shown in Fig. 7. In Models I and II, τ increases almost monotonically from zero to the yield pressure of circumferential bars. At higher pressure level where almost all of the circumferential bars reach the yield point, further resistance capacity of these bars against lateral pressure does not remain. Then, base shear stress of wall end increases rapidly until failure. In case of pressure test under thermal effects ΔT_d , (See Fig. 4) the initial residual base shear stress before pressurizing is approximately equal to 14 kg/cm². If the superposition principle of stresses holds effective, this base shear stress might increase with pressure. However, as shown in Fig. 7 the shear stress remains unchanged with respect to increase in pressure level. This result can be explained as follows: thermal component of base shear stress, τ_t , decreased with the rigidity of shell wall which reduced rapidly by cracking formation. Thus, the total shear stress $\tau = \tau_p + \tau_t$ does not increase with pressure. Residual shear stress reduces with the yield of circumferential bars which develop from top to wall end.

5. Nonlinear Axisymmetric Finite Element Analysis

A nonlinear finite element analysis has been applied to analyze test Models II and III. The analytical method is an iterative procedure for incremental loading accounting for tensile stress of concrete between cracks. Therefore, the average rigidity being reduced by cracking formation does not immediately reach that of reinforcement. Relationship between tensile stress and strain of concrete is assumed as shown in Fig. 8. For estimating the rigidity of cracked member the basic equation proposed by CEB-FIP Model Code [4] is used. Bi-linear stress and strain characteristic of reinforcement is adopted.

6. Model for Analysis and Discussions

The finite element mesh of test model is shown in Fig. 9 where circumferential and vertical bars are simulated to two types of thin plate elements which have rigidity only for each direction. As to loading conditions, the following two cases were considered.

CASE I (analysis corresponding to Model II): lateral pressure increase from 2 kg/cm², where still elastic behavior will be expected under this pressure level, to 5.0 kg/cm² by

an increment of 0.2 kg/cm^2 .

CASE II (analysis corresponding to Model III): lateral pressure increase from zero to 5.0 kg/cm^2 by an increment of 0.2 kg/cm^2 under the temperature distribution measured at the test of Model III.

The analytical results of wall deformation pressure curves in Case II and hoop forces of wall under pressure are shown in Fig. 10 and Fig. 11 respectively. Elastic and nonlinear distributions of hoop forces at the pressure of 3.0 kg/cm^2 up to the yielding of reinforcements agree with experimental results fairly well.

However, beyond the pressure of yielding, nonlinear analysis estimate properly the development of yielding of circumferential bars at the lower parts of wall. By the analysis of Cases I and II, base shear stress pressure curves are calculated and shown in Fig. 12. In the analysis of Case I, the irregular point was observed in the pressure range between 2.0 kg/cm^2 and 3.0 kg/cm^2 . This is explained by the existence of unbalanced stress perpendicular to initial cracking surface which is considered in the next step of incremental loading. Some of this discrepancy could be adjusted to make the increment of pressure smaller. In the analysis of Case II, combined condition with thermal effects, relatively good agreement with experimental results is obtained. In this case, the preliminary crackings were already formed by the thermal gradients of wall section, thus, irregular point was not observed.

7. Conclusions

The conclusions obtained from the results of model tests and nonlinear finite element analysis are summarized as follows.

- (1) Ultimate base shear stress predicted by the proposed criteria of Japanese concrete containment vessels [1] has enough safety margin, comparing with test results of circular shell wall model. However, the equation which bases on push off test [3] estimates it slightly higher than experimental results.
- (2) The residual shear stress due to thermal effect ΔT_d was released remarkably with decrease of membrane rigidity of wall which was caused by crack formation under increasing pressure.
- (3) From comparison of test results between Model II and III, the influence of residual shear stress on ultimate strength and failure mode was not observed. In loading condition IV of Japanese code where safety analysis is required, it is confirmed that the residual shear stress due to thermal load can be neglected.
- (4) Results of nonlinear finite element analysis accounting for the contribution of tensile stress of concrete between cracks indicated good agreement with test results especially in the case of pressure test combined with thermal effects. It explains clearly the reduction of thermal shear stress with the increasing pressure.

References

- [1] Y. Aoyagi, O. Isobata, N. Tanaka "Design Method of Reinforced Concrete Containment Vessel (RCCV) Against Radial Shear, 5th SMIRT Conference Berlin, Germany (1979).
- [2] Y. Aoyagi et al., "Behaviour of Reinforced Concrete Containment Models under Thermal Gradient and Internal Pressure", 5th SMIRT Conference Berlin, Germany (1979).

- [3] Y. Aoyagi, et al. "An experimental approach to the design of network reinforcement against in-plane shear in reinforced concrete containments" 5th SMIRT Conference Berlin.
- [4] International System of Unified Standard Codes of Practice for Structures, CEB-FIP Model Code for Concrete Structures, 3rd Edition 1978.

Table 1. Data for model design

	Prototype	Model		
		I	II	III
Scale	1	1/12	1/12	1/12
Design pressure (kg/cm ²)	1.05	1.05	1.05	1.05
Inner diameter (cm)	4,000	333	333	333
Wall thickness (cm)	180	15	15	15
Concrete Strength (F _C) (kg/cm ²)	240	240	277	279
Vertical reinforcement (%)	1.14	1.11	0.55	0.55
Circumferential reinforcement (%)	0.88	0.88	0.88	0.88

Table 2. The summary of the experimental results

		Model		
		I	II	III
Initial bending cracking pressure of end wall (kg/cm ²)		1.25	1.6	1.2
Yield of vertical bar (kg/cm ²)		3.30	3.35	3.40
Yield of circumf. bar (kg/cm ²)		3.25	3.10	2.80
Ultimate pressure (kg/cm ²)		5.78	<4.91	<5.0
Ultimate base shear stress τ _B (kg/cm ²)		20.3	<14	<18
Ultimate shear stress proposed eq. of CCV Code Mτ _u (kg/cm ²)	*	10.4	10.4	10.4
τ _B /Mτ _u		1.95	1.35	1.73
Ultimate shear stress by eq. from push off tests Eτ _u (kg/cm ²)	**	24.1 θ = 28°	17.6 θ = 28°	17.6 θ = 28°
τ _B /Eτ _u		0.84	0.79	1.02
Failure mode		failure of hoop bars	just before failure of hoop bars	just before failure of hoop bars

*) [1] $M\tau_u = 10P_H f_y / [13.2(x-0.5)/\sqrt{x} - x]$

***) [3] $E\tau_u = [0.05P_V f_y \sin^2 (70^\circ - \theta) + 0.5] \sqrt{F_C}$

where P_H : circumferential steel ratio
P_V : vertical steel ratio
f_y : yield strength of steel
x = radius of shell wall/wall thickness

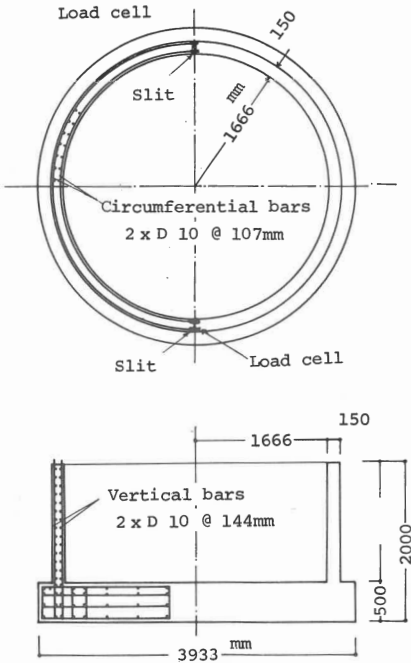


Fig. 1 Test model and arrangement of reinforcement

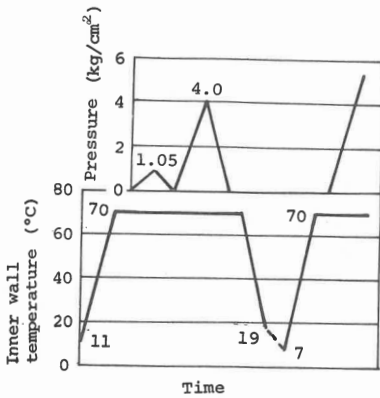


Fig. 3 Loading program

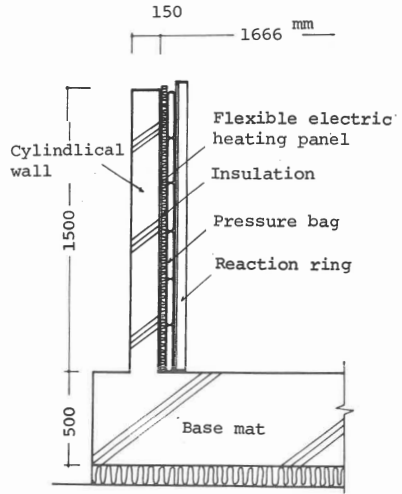


Fig. 2 Test equipment for pressure and heating

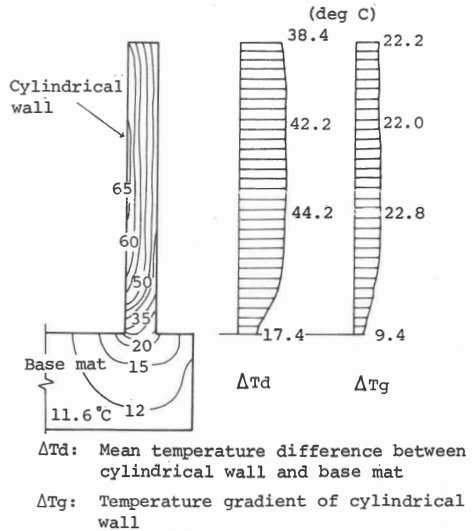


Fig. 4 Temperature distribution of Model III at pressure test

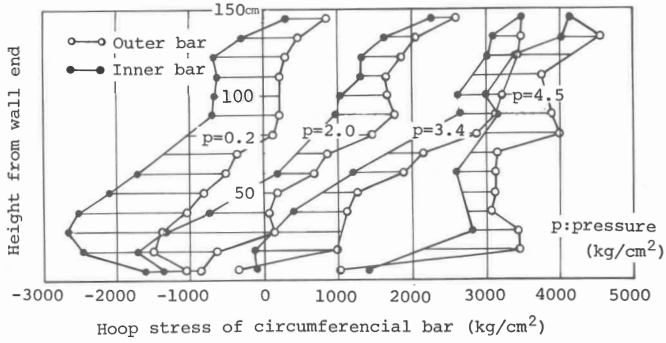


Fig. 5 Measured hoop stress of circumferential bar in Model III

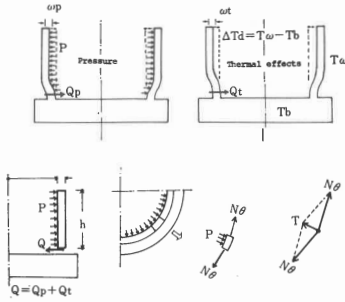


Fig. 6 Equilibrium of radial shear stress at wall end

- ① Pressure test (Model I)
- ② Pressure test (Model II)
- ③ Pressure test under thermal effects (Model III)

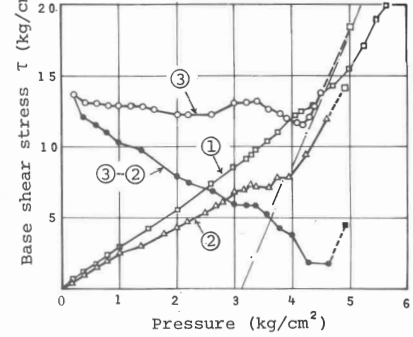


Fig. 7 Relation between pressure and base shear stress

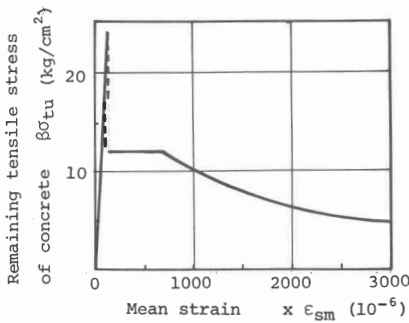


Fig. 8 Assumption on remaining tensile stress strain curve of concrete

Note:

$$\beta\sigma_{tu} = \frac{2k\sigma_{su}}{E_s \epsilon_{sm} + \sqrt{(E_s \epsilon_{sm})^2 + 4k\sigma_{sr}^2}}$$

E_s : Young's modulus of steel ($= 2.1 \times 10^6$ kg/cm²)

σ_s, ϵ_s : stress and strain of reinforcement at a cracked section

σ_{sr} : stress σ_s immediately after the cracks were formed

ϵ_{sm} : mean strain of reinforcement $\epsilon_{sm} = \epsilon_s (1 - k \frac{\sigma_{sr}}{\sigma_s})^2$

σ_{tu} : tensile strength of concrete ($= 24$ kg/cm²)

k : constants different from the loading condition or arrangement of concrete ($= 0.5$)

β : ratio of average tensile stress to the tensile strength of concrete

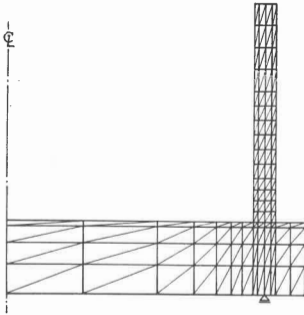


Fig. 9 Finite element mesh for nonlinear analysis

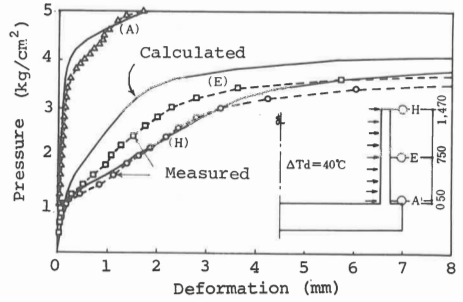
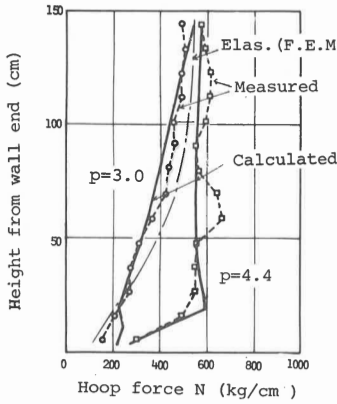
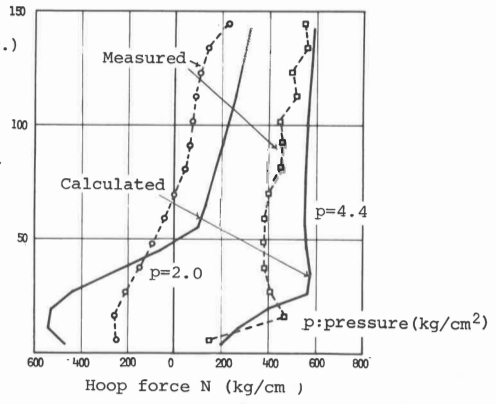


Fig. 10 Pressure deformation curve of cylindrical wall



Case I (Model II)



Case II (Model III)

Fig. 11 Comparison between measured and calculated hoop forces of cylindrical wall

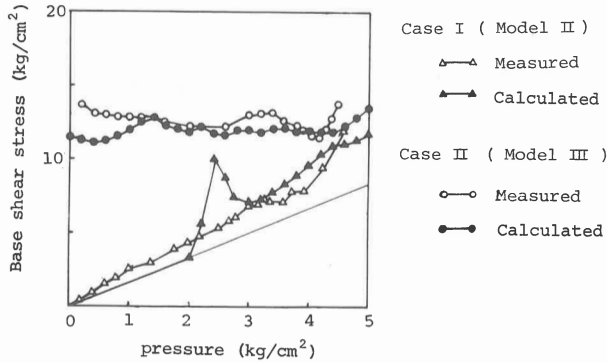


Fig. 12 Comparison between measured and calculated base shear stress of wall end

